# Palaeoenvironmental records from the West Antarctic Peninsula drift sediments over the last 75 ka

MARYLINE J. VAUTRAVERS[1]*, DAVID A. HODELL[1], JAMES E. T. CHANNELL[2], CLAUS-DIETER HILLENBRAND[3], MIKE HALL[1], JAMES SMITH[3] & ROBERT D. LARTER[3]

[1]*Department of Earth Sciences, Godwin Laboratory for Palaeoclimatic Research, University of Cambridge, Downing Street, Cambridge CB2 3EQ, UK*

[2]*Department of Geological Sciences, University of Florida, PO Box-112120, Gainesville, FL 32611, USA*

[3]*British Antarctic Survey, High Cross, Madingley Road, Cambridge CB3 0ET, UK*

**Corresponding author (e-mail: mv217@cam.ac.uk)*

**Abstract:** We present results of a multi-proxy study on marine sediment core JR179-PC466 recovered from the crest of a sediment drift off the West Antarctic Peninsula at approximately 2300 m water depth. The 10.45 m-long core consists dominantly of glaciomarine terrigenous sediments, with only traces of calcium carbonate (<1 wt%). Despite the very low abundance of calcareous foraminifera, planktonic shell numbers are sufficient for stable isotope analyses in two-thirds of the samples studied. The core chronology is based on oxygen isotope stratigraphy and correlation of its relative palaeomagnetic intensity (RPI) with a stacked reference curve. According to the age model, core PC466 spans the last 75 ka, with average sedimentation rates of between about 4 and 25 cm ka$^{-1}$. Planktonic foraminifera abundances fluctuate between 0 and 30 individuals per gram throughout the core, with minima observed during Marine Isotope Stage (MIS) 2 (14–29 ka before present, BP) and MIS4 (57–71 ka BP). Planktonic foraminifera are present in the Holocene but more abundant in sediments deposited during MIS3 (29–57 ka BP), owing to less dilution by terrigenous detritus and/or better carbonate preservation. During MIS3, foraminifera maxima correlate with Antarctic warming events as recorded in the $\delta^{18}O$ signal of the EPICA Dronning Maud Land (EDML) ice core. They indicate higher planktonic foraminifera production and better carbonate preservation west of the Antarctic Peninsula during that time. The abundance of ice-rafted detritus (IRD) in core PC466 increased during the last deglaciation between about 19 and 11 ka BP, when numerous icebergs drifted across the core site, thereby releasing IRD. During this time, sea-level rise destabilized the Antarctic Peninsula (APIS) and West Antarctic (WAIS) ice sheets that had advanced onto the shelf during the sea-level lowstand of the Last Glacial Maximum (LGM; *c.* 19–23 ka BP). Overall, our results demonstrate that it is possible to establish an age model and reconstruct palaeoceanographical and climatic changes at high temporal resolution from sedimentary sequences recovered at 2300 m water depth from a West Antarctic drift.

Mercer (1978) warned of the potential consequences of warming caused by anthropogenic greenhouse gas forcing on the stability of the West Antarctic Ice Sheet. Since the late 1970s, there has been intense scientific and public interest in the potential response of the Antarctic Peninsula Ice Sheet and West Antarctic Ice Sheet to global warming (e.g. Bindschadler 2006; Mayewski *et al.* 2009). Recent observations show that both ice sheets are undergoing rapid changes, including surface warming, ice shelf melting, flow acceleration, outlet glacier thinning and grounding-line retreat, and contribute to present sea-level rise (Vaughan *et al.* 2003; Martinson *et al.* 2008; Pritchard *et al.* 2009, 2012; Joughin & Alley 2011). These recent changes can be understood in a longer geological context by studying continuous, ice-sheet-proximal marine sedimentary records. Although numerous marine sediment cores have been recovered from the West Antarctic continental margin throughout the last 50 years, their predominantly terrigenous composition and lack of foraminiferal carbonate for isotopic analyses has hindered the establishment of precise age models and stymied palaeoenvironmental interpretations.

Here we present results of a multi-proxy study on core PC466 recovered from Sediment Drift 4 on the upper continental rise west of the Antarctic Peninsula (number according to Rebesco *et al.* 2002). The core site lies at a relatively shallow

*From*: Hambrey, M. J., Barker, P. F., Barrett, P. J., Bowman, V., Davies, B., Smellie, J. L. & Tranter, M. (eds) *Antarctic Palaeoenvironments and Earth-Surface Processes*. Geological Society, London, Special Publications, **381**, http://dx.doi.org/10.1144/SP381.12 

water depth of approximately 2300 m, where carbonate ion concentrations are high enough that sedimented calcareous particles should be preserved (e.g. Hillenbrand *et al.* 2003) and thus permit stable isotopes analysis of foraminifera. We also used the RPI of core PC466, which should reflect the variations of Earth's magnetic field, as a stratigraphical tool (Sagnotti *et al.* 2001; Macrì *et al.* 2006; Venuti *et al.* 2011).

In this study, we aim to assess the feasibility of reconstructing the Late Quaternary environmental history of the Antarctic Peninsula region by analysing marine sediments from the continental rise that are low in biogenic calcium carbonate. The specific objectives are to: (1) develop an accurate age model for core PC466; (2) infer ice-sheet dynamics (e.g. advance and retreat); and (3) reconstruct changes in surface water conditions, such as sea-surface temperature and sea-ice cover. Although the methods employed are relatively standard at lower latitudes, it is more challenging to apply them in the Antarctic environment. We first evaluate how well each proxy performed and then discuss the inferred palaeoenvironmental history in the final section.

## Study area

The surface water current regime on the western Antarctic Peninsula shelf is characterized by a cyclonic gyre. The Antarctic Circumpolar Current (ACC) and the shelf gyre are separated by the southern boundary of the ACC, a front that runs along the shelf break (Orsi *et al.* 1995). As a result of this circulation pattern, some icebergs calved from the Antarctic Peninsula Ice Sheet and the West Antarctic Ice Sheet into the Bellingshausen and Amundsen seas drift clockwise towards the shelf (e.g. Gladstone *et al.* 2001), whereas others may be carried further east through the Drake Passage by the ACC (Young 1998).

The water masses in the study area are from top to bottom: (1) fresh and very cold (near-freezing temperature) Antarctic Surface Water; (2) Upper Circumpolar Deep Water (UCDW), which is characterized by an oxygen minimum and maximum in nutrients and temperature (Ito *et al.* 2010); and (3) relatively warm and salty Lower Circumpolar Deep Water (LCDW), which is a remnant of North Atlantic Deep Water (NADW) input to the ACC, and Weddell Sea Deep Water (WSDW). While most of the LCDW and UCDW are affected by the ACC, the bottom water on the uppermost continental rise, where core PC466 was taken, consists of SW-flowing modified WSDW and LCDW (Withworth *et al.* 1998; Hillenbrand *et al.* 2008*b*).

The annual average sea-surface temperature (SST) near the site of PC466 is about 0 °C (Locarnini *et al.* 2006), and the surface water salinity is lower than 34‰, owing to the winter sea ice maintaining a strong halocline (Antonov *et al.* 2006). The site is located slightly south of the Polar Front (Dong *et al.* 2006) and covered by sea ice for about 4 months each year (Parkinson 2004). The study area has the largest extra-tropical SST response to El Niño Southern Oscillation (ENSO) on Earth (Yuan 2004), with ENSO having a large impact on the annual sea-ice cover (Kwok & Comiso 2002). During the last 60 years, the area has experienced rapid and major amplified anthropogenic warming, with a summer SST increase of up to 1 °C (Meredith & King 2005). The surface water salinity has also increased, while the winter sea-ice concentration has decreased (Vaughan *et al.* 2003).

Biological productivity at the core site occurs mainly during the approximately 8 months of open water in spring and summer, although some primary production (sea-ice diatoms) takes place within the sea ice (Arrigo *et al.* 1998). The planktonic foraminifer species of *Neogloboquadrina pachyderma* sinistral is able to survive in sea-ice cavities and brine channels (Dieckmann *et al.* 1991). Consequently, as elsewhere in the Antarctic marginal ice zone, particle flux in the water column exhibits a high seasonality, with a strong maximum in summer following the sea-ice retreat and the phytoplankton bloom (Wefer *et al.* 1988; Ducklow *et al.* 2008). Species distribution and community composition of the plankton are tightly correlated with water masses, oceanic fronts and the sea-ice edge (Ducklow *et al.* 2007).

The Antarctic Peninsula Ice Sheet is less than 500 m thick (Drewry 1983). Along its western margin, this ice sheet terminates in steep margins and tidewater glaciers. The Antarctic Peninsula Ice Sheet is thicker in the east, where it drains via glaciers and larger ice shelves into the Weddell Sea. During the LGM, the Antarctic Peninsula Ice Sheet and West Antarctic Ice Sheet advanced across the shelf (Anderson *et al.* 2002; Livingstone *et al.* 2012; Davies *et al.* 2012), and grounded ice streams advanced to the shelf break adjacent to Sediment Drift 4 (see references in Livingstone *et al.* 2012) (Fig. 1). The sedimentary changes on drifts west of the Antarctic Peninsula during the Late Quaternary have been described previously by Pudsey & Camerlenghi (1998), Pudsey (2000), Hillenbrand & Ehrmann (2003), Lucchi *et al.* (2002) and Lucchi & Rebesco (2007) but these studies were hindered by the lack of robust age models.

## Core material

Piston core PC466 was recovered during expedition JR179 aboard the RRS *James Clark Ross* in 2008.

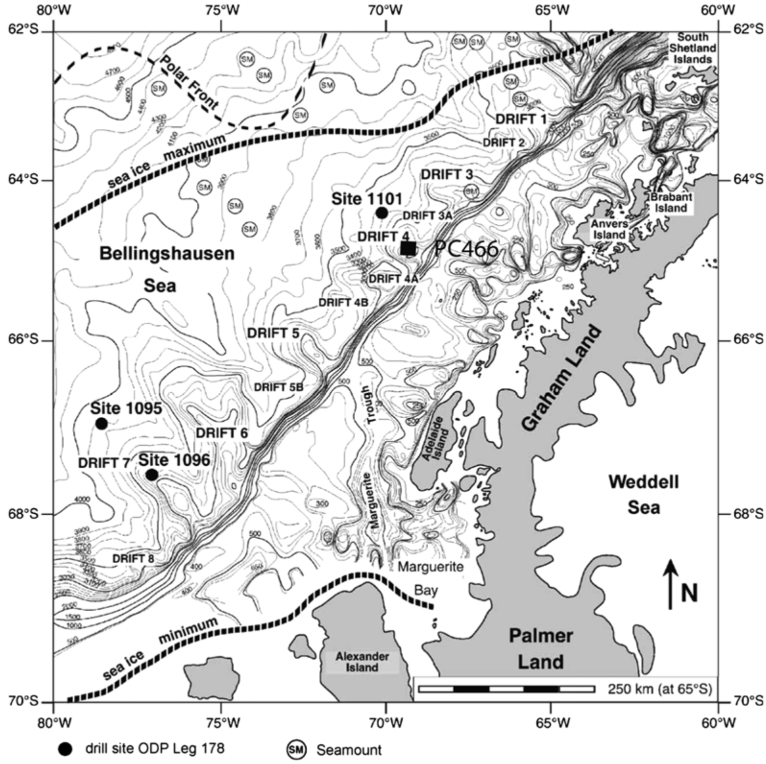


**Fig. 1.** Regional oceanographical map showing the core site (PC466, black square) on Sediment Drift 4 and previous continental rise drilling sites of Ocean Drilling Program (ODP) Leg 178 (reproduced from Hillenbrand & Ehrmann 2005). Extent of existing ice shelves around the Antarctic Peninsula is not represented on the map.

The 10.45 m-long core is located at 64°54′.60 S and 69°04′.59 W, at a water depth of 2306 m. Core PC466 contains two lithological units: the upper Unit I (0–57 cm) consists of bioturbated olive mud; whereas the lower Unit II (57–1045 cm) consists mainly of homogeneous, occasionally finely laminated, greyish–brownish mud with rare occurrence of thin sand layers and sand lenses. We also investigated a few samples from the 1.12 m-long trigger core TC466 collected at the same location. TC466 recovered grey–olive muds, which are bioturbated (0–47 cm) and homogeneous (47–112 cm), respectively.

## Methods

### *Magnetic sediment properties*

The relative palaeo(magnetic) intensity (RPI) (Fig. 2b) was obtained for each u-channel sample, natural remanent magnetization (NRM) components were determined at 1 cm spacing and demagnetized at 5 mT steps in the 10–100 mT peak field range. Anhysteretic remanent magnetization (ARM) was acquired in a peak alternating field of 100 mT and a 50 μT DC bias field. ARM was measured prior to and after demagnetization at 5 mT steps in the 10–60 mT peak field range. The relative strength of the magnetizing field or RPI can be determined by using the intensity of ARM to normalize the NRM intensity for changes in concentration of remanence-carrying grains. The resulting normalized remanence, calculated as the slope of the NRM-intensity v. ARM-intensity in the 20–60 mT peak field range, is a proxy for RPI variations and can be correlated to a calibrated palaeointensity template (reference curve) produced by stacking several independently-dated RPI records (e.g. the ‘PISO-1500’ stack: Channell *et al.* 2009) to produce the age model. The volume magnetic susceptibility data (Fig. 2b) were measured on u-channels at 1 cm intervals using a custom-built instrument at the University of Florida (Thomas *et al.* 2003). The 3.3 cm square coil of this instrument has a narrow response function (*c.* 3 cm half-peak width) designed to maximize measurement resolution.

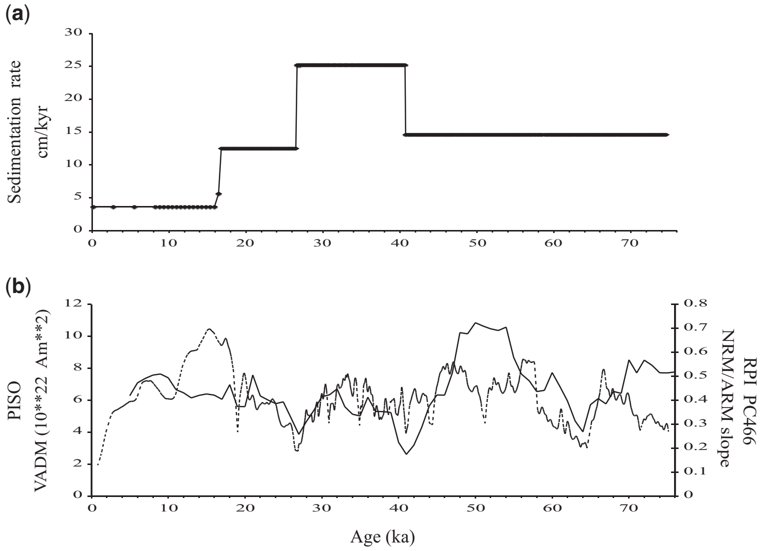


**Fig. 2.** Stratigraphy and sedimentation rate in core PC466 from relative palaeointensity (RPI) stratigraphic tie-lines (Table 1). (**a**) Sedimentation rate in cm/ka. (**b**) core PC466 RPI record based on the slope of the NRM intensity v. ARM intensity in the 20–60 mT peak field demagnetization range (dash line) compared to the PISO RPI reference curve (Channell *et al.* 2009) scaled to virtual axial dipole moment (VADM) (solid black line).

## Sampling and processing

The core was systematically sampled by taking approximately 5 cm$^3$ of 1 cm-thick slices at 2 cm intervals. Carbonate content was determined on 68 bulk sediment samples. Total inorganic carbon was determined by acidification using an AutoMateFX carbonate preparation system, and evolved $CO_2$ was measured using a UIC Coulometrics$^{TM}$ 5011 $CO_2$ coulometer. Weight per cent calcium carbonate ($CaCO_3$, %) was calculated by multiplying the values of total inorganic carbon by 8.33 (the ratio of molecular weight of $CaCO_3$ to C). All samples were dispersed in approximately 50 ml of de-ionized water, then placed for 2 h on a rotating table and, afterwards, were wet sieved through a 63 μm mesh using a gentle spray of de-ionized water using 500 ml of water. The coarse fraction was dried on the sieve in an oven at less than 50 °C and then weighed. The fine fraction was left to settle for up to 2 days and then dried, weighed and retained for grain size analysis.

## Coarse fraction examination

### Microfossil content

Each >63 μm sample was dry sieved over a 150 μm mesh. The entire >150 μm fraction of each sample was placed on a gridded tray for quantitative examination under a binocular light microscope. All planktonic foraminifera, fragments of planktonic foraminifera, radiolaria, ostracodes and benthic foraminifera (calcareous or agglutinated) were counted in the whole >150 μm fraction. We distinguished and counted two morphotypes of *N. pachyderma* (s) (Fig. 3a, b). The most frequent morphotype A is square shaped with a secondary crust showing various stages of preservation and is often relatively large. Morphotype B has a more lobate shape and thinner shell than morphotype A. In the Arctic, the low proportion of morphotype B in sediments and its high proportion in the water column suggest (Vilkes 1975) that it is the juvenile form of morphotype A, which is consistent with the lack of gametogenic calcite encrustation and the often smaller test size of morphotype B.

### Lithogenic content

The >63 μm fraction was dry sieved over a 355 μm sieve, and all terrigeneous particles in the fraction >355 μm were counted as ice-rafted detritus (IRD). Rare large drop-stones (>0.5 cm and >1 cm) were counted separately. Ice-rafted detritus abundance is expressed in grain numbers per gram of dry sediment.

### Stable isotopes and trace metal analyses

Because the samples from core PC466 contain only a few calcareous benthic foraminifera tests,

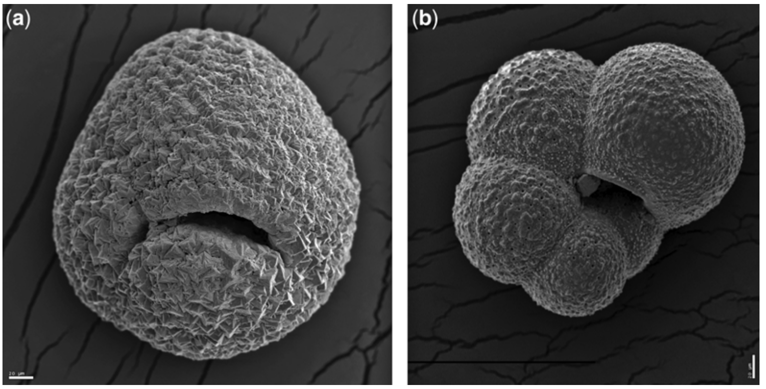


**Fig. 3.** Morphotypes of *N. pachyderma* (s). (**a**) Adult (encrusted) specimen of *N. Pachyderma* (s) taken from a sample at 1000 cm depth in core PC466. (**b**) Juvenile specimen *N. Pachyderma* (s) taken from a sample at 800 cm depth in core PC466.

geochemical analyses were exclusively performed on *N. pachyderma* (s) morphotype A. Picking was performed once the overall number of shells available per sample was known. Most measurements for stable isotopes and all Mg/Ca analyses were carried out in the Godwin Laboratory at the University of Cambridge. Sample treatment followed standard cleaning procedures. Foraminifera shells were crushed and soaked in a solution of 3% hydrogen peroxide for 30 min in individual vials. Acetone was added and the samples placed in an ultra-sonic bath, after which the liquid was decanted carefully using a tissue. The samples were dried in an oven at 50 °C overnight. Initially, stable isotopes were analysed on 24 samples containing less than 10 individuals of *N. pachyderma* (s) in the 212–250 μm fraction using a VG PRISM mass spectrometer and MultiPrep carbonate device. A second set of 78 samples containing up to 30 specimens was measured using a VG Sira mass spectrometer and MultiPrep device. Analytical error for all these samples was ±0.06‰ for $\delta^{18}O$ and ±0.08‰ for $\delta^{13}C$. In addition, 58 samples containing only a few tests or large test fragments were prepared in Cambridge and measured at the University of Florida using a ThermoScientific MAT 252 mass spectrometer coupled to a Kiel carbonate device. Precision of these measurements was ±0.06‰ for $\delta^{18}O$ and ±0.02‰ for $\delta^{13}C$.

Twenty-four samples containing ≥17 shells in the fraction 212–300 μm were selected for trace metal analyses. Each sample was cleaned following the procedure of Barker *et al.* (2003) and analysed on a Varian Vista ICP-AES (inductively coupled plasma atomic emission spectroscope) using the intensity ratio calibration method of de Villiers *et al.* (2002). We present results as Mg/Ca ratios ($mmol \cdot mol^{-1}$) rather than SSTs, thereby interpreting relative temperature changes only. Additional data obtained from these analyses are individual shell weights, which are relevant to understand down-core changes in carbonate preservation (cf. Moy *et al.* 2009).

### *Grain size analysis*

The grain size distribution within the silt fraction was analysed on 1 g of dry sediment from the >63 μm fraction and expressed as mean sortable silt. We followed the methodology of McCave *et al.* (1995) but without the initial use of hydrogen peroxide and 0.1% sodium hexa-metaphosphate (Calgon). Even though most samples are $CaCO_3$-free, we treated the samples with dilute acetic acid (1 M) to remove all $CaCO_3$ prior to grain size analysis. We also removed biogenic opal with heated sodium carbonate (2 M). Grain sizes were analysed with a Coulter Counter Multisizer 3 after the samples had been suspended in a 0.2% Calgon and 1% NaCl isotonic solution to prevent flocculation. Particle counting was performed using 64 bins of sizes from 10 to 63 μm (the sortable silt fraction). Because PC466 was recovered from a sediment drift, we interpret variations in mean sortable silt as changes in bottom-current speed. Nevertheless, we acknowledge that the interpretation of this proxy can be more complicated in high-latitude continental margins because of the pronounced changes in IRD supply, down-slope transport and the source of the terrigenous detritus (McCave & Hall 2006).

## Results

### *Stratigraphic framework*

The age model for core PC466 is based on the integrated lithostratigraphy, oxygen isotopes and

RPI. A common lithostratigraphical succession has been documented previously in numerous cores recovered from the study area (Pudsey & Camerlenghi 1998; Pudsey 2000; Lucchi *et al.* 2002; Hillenbrand *et al.* 2008*a*): (i) MIS1 (0–14 ka BP) and MIS5e are marked by bioturbated muds containing siliceous microfossils and biogenic opal, whilst calcareous microfossils are rare to absent and $CaCO_3$ content is very low; and (ii) MIS2–MIS4 and MIS6 are marked by terrigenous, laminated to homogenous muds largely barren of microfossils. This lithostratigraphical succession was supported by chemostratigraphy (Pudsey & Camerlenghi 1998; Pudsey 2000), biostratigraphy (Villa *et al.* 2003), $^{230}Th_{excess}$ dating (Pudsey 2000), tephrochronology (Hillenbrand *et al.* 2008*a*) and RPI dating (Macrì *et al.* 2006; Venuti *et al.* 2011). Applying this lithostratigraphy to core PC466, Unit I corresponds to MIS1, whereas Unit II corresponds to MIS2–MIS4. The basal stage assignment of the core to MIS4 is supported by the absence of tephra layers in Unit II, which were deposited at nearby core sites during MIS5e (Hillenbrand *et al.* 2008*a*). The $\delta^{18}O$ data on *N. pachyderma* (s) from core PC466 suggest that the boundary between MIS1 and MIS2 (Termination I) lies somewhere between about 30 and 135 cm core depth. Three lows recognized in the RPI record from core PC466 can be correlated to minima in the 'PISO' stack at 25, 40 and 64 ka (Fig. 2b). The age model for core PC466 (Table 1) was constructed and sedimentation rates estimated using the three RPI tie points, and assuming that the top of the core is modern (Fig. 2a).

## *Stable isotope results*

Beyond the general aim of producing a stratigraphy based partly on oxygen isotopes, we also wanted to test whether the sediments at this site contain sufficient foraminifera to generate meaningful palaeoenvironmental records.

In the upper part of core PC466, only three samples from 1 to 30 cm below sea floor (cm b.s.f.) contained enough specimens for isotope analyses, and they all yielded low $\delta^{18}O$ values (Fig. 5c) ranging between 3.3 and 3.4‰, which are consistent with core top values from the region (e.g. Mulitza *et al.* 2004) and comparable to those of Holocene sediments from the Bellingshausen Sea (e.g. Hillenbrand *et al.* 2010). In contrast, $\delta^{18}O$ values in samples below 136 cm b.s.f. to the base of core PC466 vary between approximately 4.7 and 5.2‰, and thus resemble values reported from *N. pachyderma* (s) in Antarctic continental margin sediments deposited during MIS2–MIS 4 (e.g. Mackensen *et al.* 1994; Rickaby *et al.* 2010). The planktonic $\delta^{18}O$ signal of PC466 does not allow a distinction between MIS4, MIS3 and MIS2 by itself. Planktonic $\delta^{13}C$ values (Fig. 6d) decrease slightly from a value of approximately 0.2 to about 0.0‰ from 74 to 64 ka, and increase to approximately 0.4‰ from 58 to 23 ka. After a gap in the record during Termination I, they reach a maximum of about 0.8‰ at 3 ka. Throughout MIS4–MIS3, fluctuations of about 0.4‰ are superimposed on the longer-term changes.

A continuous stable isotope record could not be obtained because foraminifera are very rare during the Holocene (less than 1 per gram), virtually absent during MIS2 and rare during MIS4.

## *Sedimentological results*

Weight per cent $CaCO_3$ ranges from below detection limits to approximately 1 wt%, showing a general decrease up-core (Fig. 5d). Although the carbonate concentrations are close to the analytical error of the measurements (+ to −0.5 wt%), the variations in wt% $CaCO_3$ are supported by abundant variations of planktonic foraminifera.

The coarse fraction (>63 μm) contains, on average, only two foraminifera specimens per g of dry sediment (Fig. 4e). Thus, this fraction is mainly a proxy for the coarse lithogenic material. The fraction >63 μm tends to increase when the mean sortable silt decreases and, therefore, suggests that these variations are primarily related to IRD supply rather than to gravitational down-slope transport. The average percentage of the >63 μm fraction throughout core PC466 is only 2.6 wt%, with a maximum of 20.6% found during the last deglaciation at 11.2 ka. In contrast, values of about 0% occur during the LGM and middle Holocene.

In general, the fluctuations of IRD concentration (Fig. 4d) coincide with variations in the >63 μm fraction. Ice-rafted detritus particles >355 μm are found in 519 of the 538 samples examined, underscoring the fundamental influence of IRD deposition at this site. The average IRD content is approximately 5 grains/g. The maximum is 163 grains/g and found at the top of TC466.

In some intervals, the magnetic susceptibility (MS) is negatively correlated with the content of large lithogenic particles (Fig. 4c, d); for example, the MS minima at the MIS4–MIS3 transition is rich in larger particles. For all the intervals with low amounts of IRD larger than 0.5 cm (for example, during the earlier part of MIS3), a good correspondence exists between the contents of the fraction >63 μm and the MS. This suggests that, for these intervals, the grains responsible for the MS signal are concentrated in the fine sand fraction >63 μm. An examination of large IRD grains deposited during the last deglaciation and the MIS4–MIS3 transition revealed that they are composed of metamorphic rock fragments (gneiss, mica schist, green schist).

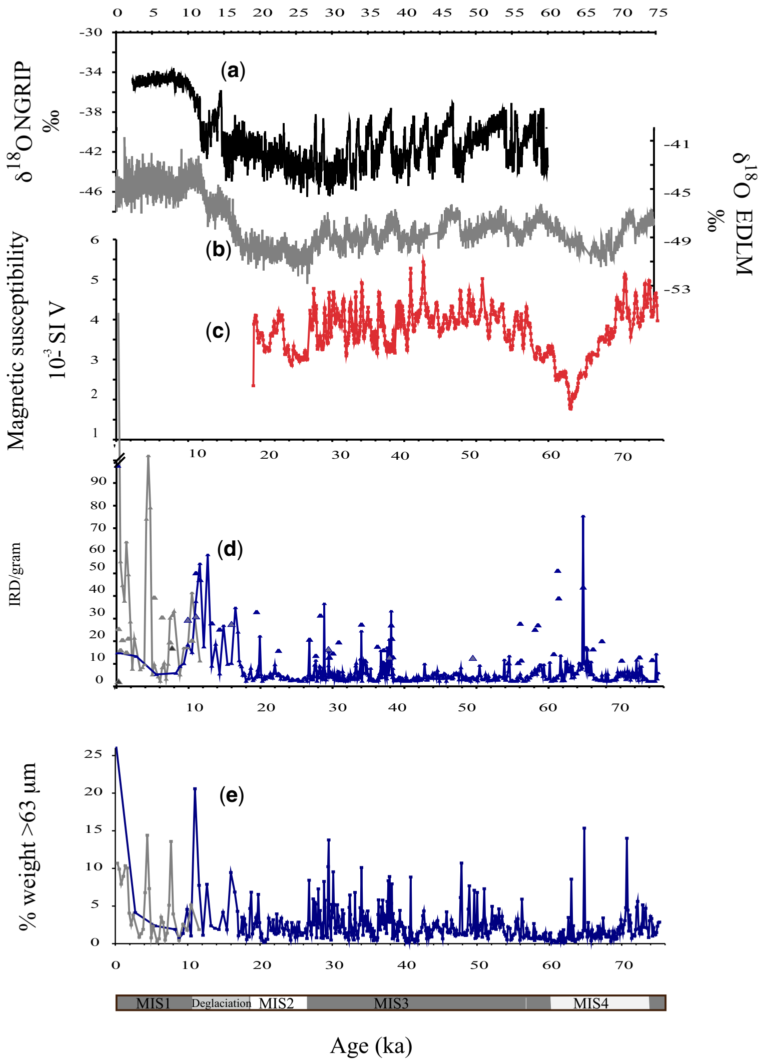


**Fig. 4.** The lithogenic records of core PC466. (**a**) Ngrip $\delta^{18}O$ (‰) Rasmussen *et al.* 2008. (**b**) EDML $\delta^{18}O$ (‰) (EPICA Community Members 2006). (**c**) Magnetic susceptibility. (**d**) IRD $> 335$ µm (lines, blue PC466, grey TC466). Medium triangles are for IRD $> 0.5$ cm and large triangles for IRD $> 1$ cm. (**e**) Percentage of fraction larger than 63 µm (lines, blue PC466, grey TC466).

**Table 1.** *Stratigraphical tie points**

| Depth in core (cm) | Age BP (ka) |
|---|---|
| 0 | 0 |
| 61 | 16.8 |
| 186 | 26.8 |
| 544 | 41 |
| 880 | 64 |

*Depth (cm in core) and ages (ka) used in the correlation between the PC466 RPI and the 'PISO' RPI reference curve (Fig. 2).

The mean sortable silt (Fig. 6c) fluctuates between 15.4 and 26.6 µm (average 18 µm), and shows some positive correlation with the MS (Fig. 2c), which itself is anti-correlated with the concentration of IRD >335 µm (Fig. 4d).

## *Microfossil content*

The planktonic foraminifera content of 405 out of 538 samples is at least of one whole shell of the planktonic foraminifera species *N. pachyderma* (s).

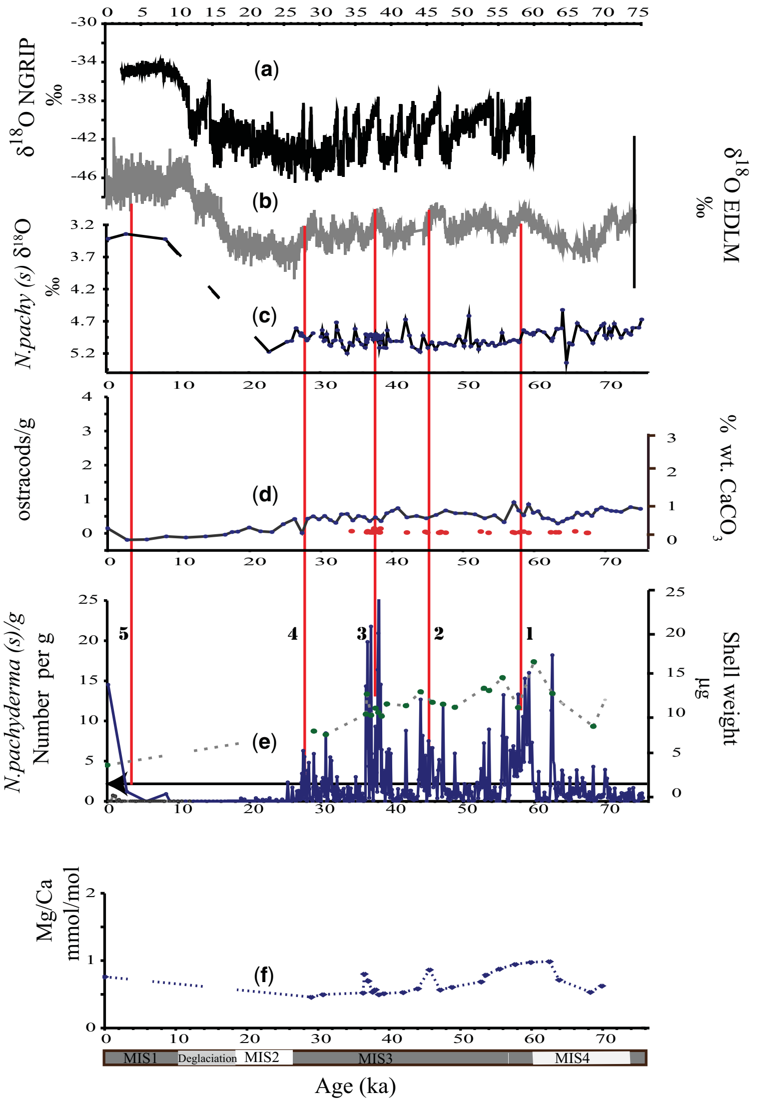

**Fig. 5.** Coarse fraction biogenic components v. $\delta^{18}O$ (‰). (**a**) Ngrip $\delta^{18}O$ (‰) Rasmussen *et al*. 2008. (**b**) EDML $\delta^{18}O$ (‰) EPICA Community Members, 2006. (**c**) $\delta^{18}O$ (‰) measured on *N. Pachyderma* (s). (**d**) Number of ostracods valves per gram of dry sediment (red dots). % wt $CaCO_3$ line with dots. (**e**) Number of *N. pachyderma* (s) per gram of dry sediments. Horizontal solid line is average *N. Pachyderma* (s) per gram. Dotted line with green dots is for shell weight in µg. (**f**) Mg/Ca measured on *N. Pachyderma* (s).

Maximum abundances are only 30 specimens per g, and occur at about 36 ka (Figs 5e & 6f). The average content for all samples is below two specimens per g of dry sediment. This is a very small amount considering that a more typical range of shells concentrations in deep marine sediments at 2500 m depth (outside polar area) is between a few hundred and a few thousand tests per g of dry sediments. We recognize five intervals with foraminifer concentrations above the average of two specimens per g: between 62 and 56 ka; between 50 and 43 ka: between 40 and 35 ka: between 32 and 27 ka: and from 8 to 0 ka. These intervals appear to correlate with warming events recorded in Antarctic ice cores, such as those expressed in the $\delta^{18}O$ record of the EPICA Dronning Maud Land ice core (EPICA Community Members 2006). Unexpectedly, a few samples

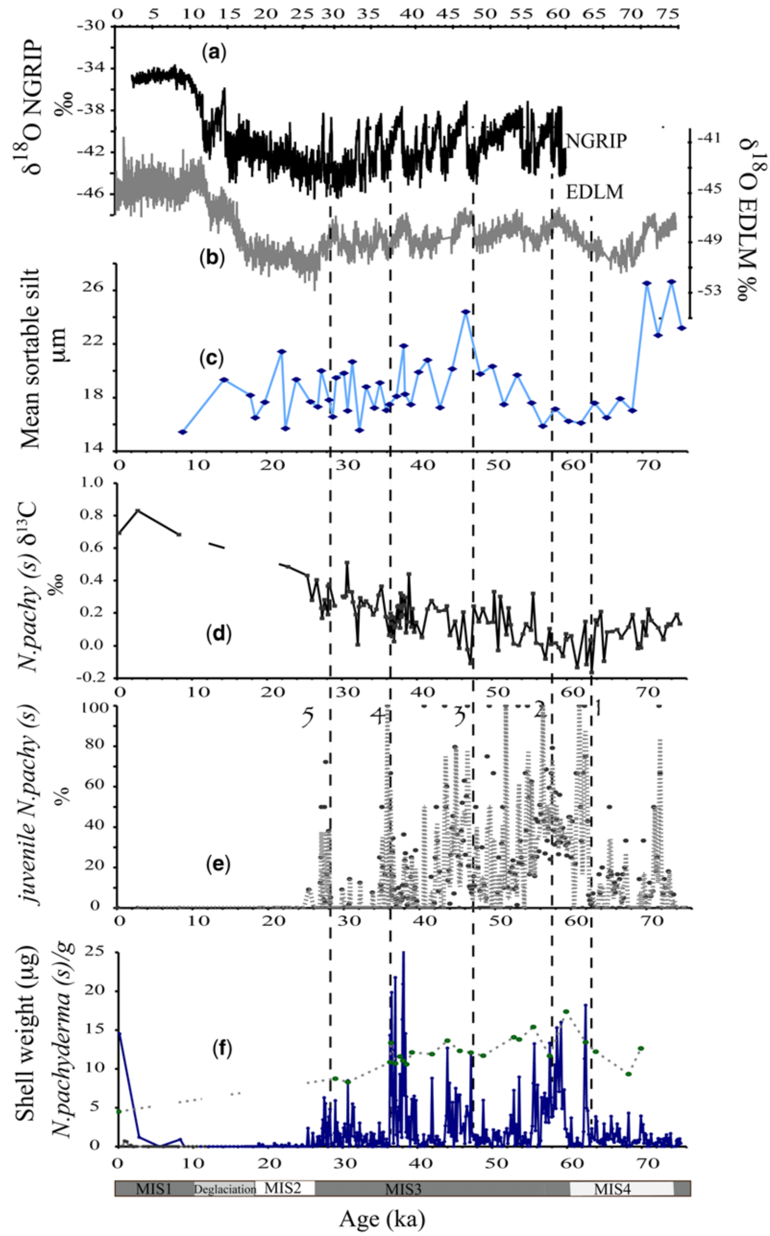


**Fig. 6.** Sea ice and paleocirculation records. (**a**) Ngrip $\delta^{18}O$ (‰) Rasmussen *et al*. 2008; (**b**) EDML $\delta^{18}O$ (‰) EPICA Community Members, 2006; (**c**) Mean Sortable Silt in mm as a proxy of deep-current speed; (**d**) $\delta^{13}C$ (‰) measured on *N. Pachyderma* (s); (**e**) Percentage of juvenile morphotype (B) of *N. pachyderma* (s) (see Fig. 3) in total *N. pachyderma* (s): dots. The grey line is the smooth curve (2 points moving average). 1 to 5 refer to 5 peaks of representation; (**f**) Reproduced from Figure 5 for visual reference: Number of *N. pachyderma* (s) per gram of dry sediments Horizontal solid line is average *N. Pachyderma* (s) per gram. The dotted line with green dots is for shell weight in µg.

(18 out of 538) contained a few specimens of planktonic foraminifera other than *N. pachyderma* (s), indicating even warmer surface waters.

Trace metals analyses reveal that the highest Mg/Ca ($0.98\ \mathrm{mmol \cdot mol^{-1}}$) values occurred between 64 and 58 ka and the lowest ratios at

25 ka (0.46 mmol · mol$^{-1}$) (Fig. 5f). Mg/Ca ratios are 0.76 mmol · mol$^{-1}$ in the core-top sample, which is lower than most of the peak Mg/Ca values observed during MIS3.

The thinned-shell *N. pachyderma* (s) morphoptype B (Fig. 6e), which is abundant between 72 and 26 ka, is less resistant to dissolution than the heavily encrusted morphotype A. We assume that morphotype B represents a juvenile form of morphotype A and its abundance may increase when the sea-ice cover increases. A simple explanation might be that the relative increase of morphotype B is the result of premature death of the few young specimens present at the time of sea-ice formation before they could grow and develop into encrusted adults and reproduce.

For all the samples selected for Mg/Ca (*N. pachyderma* (s), morphotype A) an average shell weight (Fig. 6f) was obtained for samples with at least 10 shells in the 212–300 μm size range. Average shell weight ranges from 4.5 μg during the Holocene to just above 17 μg at 62 ka. In addition, shell weight declines from 62 to 25 ka, in parallel with the $CaCO_3$ content. Decreases in average shell weight are interpreted to represent increasing calcium carbonate dissolution.

Benthic foraminifera in the >150 μm fractions are extremely rare and are present in only 126 samples out of 538 samples. Examination of the fraction below 150 μm for a few samples shows that benthic foraminifera are always extremely small. Agglutinated foraminifera >150 μm (counted as a whole group) are mainly restricted to the Holocene where they dominate the benthic assemblage (between three and 20 specimens per sample).

Finally, we note the rare but remarkable occurrence of a few well-preserved ostracods valves (Fig. 5d) in a few samples clustering around 58 and 38 ka.

## Discussion

The development of a coherent age model for core PC466 permits the suite of multi-proxy records to be interpreted in terms of temporal changes in oceanic surface conditions (e.g. temperature, sea-ice cover and influence of icebergs). The results are discussed chronologically in five time intervals: MIS4 (74–60 ka); MIS3 (60–24 ka); Last Glacial Maximum (24–18 ka); the Last Deglaciation (18–11 ka); and MIS1 (11–0 ka) or Holocene. All intervals are shown in Figures 4, 5 and 6.

Carbonate content and foraminiferal abundance was greater during MIS4 than the LGM (MIS2), suggesting that sea-ice cover may have been less extensive during the penultimate glaciation. This interpretation is consistent with evidence for lower sea-salt concentrations in Antarctic ice cores during MIS4 than MIS2, which has been used as a proxy for Southern Ocean sea-ice cover (Wolf *et al.* 2006).

During MIS4 and MIS3, the planktonic $\delta^{18}O$ signal in core PC466 (Fig. 5c) is marked by low variability (*c.* 0.5‰), varying between approximately 4.7 and 5.2‰. In fact, the planktonic $\delta^{18}O$ record from core PC466 displays the subdued characteristics of a benthic $\delta^{18}O$ record during the last glacial interval. The high $\delta^{18}O$ values during MIS3 and MIS4 indicate the persistence of near-freezing temperatures and the absence of input of large amounts of isotopically-depleted meltwater at the depth inhabited by *N. pachyderma* (s) (morphotype A). Isotope analyses were conducted exclusively on morphotype A. of *N. pachyderma* (s). This morphotype has a secondary gameotgenic crust that is added between 50 and 200 m (Kohfeld *et al.* 1996), and maximum abundance of encrusted *N. pachyderma* (s) often occurs at the pycnocline. Thus, $\delta^{18}O$ of *N. pachyderma* does not reflect surface conditions but rather is biased towards the depth interval of the main pycnocline (100–200 m).

Sediments deposited during MIS3 contain the highest carbonate content and the greatest abundances of planktonic foramifera. Enhanced carbonate preservation is supported by the presence of the fragile morphotype B of *N. pachyderma* (s) during MIS3, high shell weight for *N. pachyderma* (s), and the rare occurrence of a few ostracods carapaces close to 58 and 38 ka. According to our age model, four peaks of foraminiferal abundance occurred during MIS3: between 62 and 56 ka; between 50 and 43 ka; between 40 and 35 ka; and between 32 and 27 ka.

Increases in the wt% of carbonate and the planktonic foraminiferal abundances can result from: (i) increased biological carbonate productivity in surface waters; (ii) less carbonate dissolution; and/or (iii) decreased dilution by non-carbonate material (e.g. terrigenous). The four peaks in carbonate and planktonic foraminifera during MIS3 are reminiscent of four warming events (A1–A4) recorded in Antarctic ice cores during MIS3 (EPICA Community Members 2006). Whilst it is tempting to attribute the increased foraminiferal abundances to decreased sea-ice cover during these warming events, four peaks in carbonate preservation have also been identified in the deep Indian (Mleneck-Vautravers 1997) and South Atlantic oceans (Kanfoush *et al.* 2000). These carbonate events occur just after the Antarctic warm events and are associated with increased North Atlantic Deep Water formation (Anderson & Fleisher 2011). The resolution of our age model does not permit us to resolve whether the carbonate events in PC466 are synchronous with the Antarctic warm events or occur just afterwards, and thereby correlate with increases in the deep-sea carbonate preservation.

There is no apparent change in planktonic $\delta^{18}O$ associated with times of increased abundance of *N. pachyderma,* but foraminiferal productivity may be responding to conditions at the surface, whereas $\delta^{18}O$ is biased towards calcite added at greater depth. In contrast, variations in the Mg/Ca of *N. pachyderma* indicate several apparent increases during MIS3 that coincide with increased foraminiferal abundances. Although these could indicate warmings during MIS3, they are difficult to reconcile with the lack of a $\delta^{18}O$ change. Mg/Ca can also be affected by carbonate ion concentration because calcite with higher Mg content preferentially dissolves, thereby lowering Mg/Ca. The peaks in Mg/Ca are associated with better carbonate preservation (less dissolution) that could result in higher Mg concentrations, which would be indistinguishable from increased Mg/Ca related to warming.

Despite clear fluctuations in foraminifera concentrations, which may correspond with interstadials during the early part of MIS3 (prior to 38 ka), these events are not associated with changes in IRD concentrations, suggesting that very few icebergs were being produced and/or melting at the location of PC466 during the first part of MIS3. Generally, IRD concentrations were higher after 40 ka, including the coarsest fraction of detrital grains (larger than 0.5 cm). We speculate that this IRD increase could be related to the size of the nearby APIS, which may have advanced onto the continental shelf when sea level dropped during the later part of MIS3 (e.g. Siddall *et al.* 2008). The relative early expansion of APIS during late MIS3 may have been related to reduced sea-ice cover during MIS3. Seasonally open water would have provided a source of moisture for ice growth.

Palaeoenvironmental interpretations are limited during MIS2 because of the absence of foraminifera. The persistently low concentration of IRD during the LGM may indicate: (i) the APIS was very stable; (ii) the APIS margin terminated in ice shelves; or (iii) permanent sea-ice coverage reduced the drift of icebergs to the site of PC466. The presence of perennial sea ice may also explain the lack of foraminifera, as it would have suppressed biogenic $CaCO_3$ production.

During the last deglaciation, foraminifera were also absent owing to a combination of reduced carbonate production, dissolution and/or dilution by terrigenous sediment. Ice-rafted detritus concentrations reached a maximum during the last deglaciation, beginning at 18 ka BP and continuing until 10 ka BP. This onset of the last deglaciation at the site of PC466 occurred synchronously with the initial APIS retreat from the outer continental shelf (e.g. Livingstone *et al.* 2012), but 3–4 ka earlier than estimated by Clark *et al.* (2009) according to the age model of the core. Once the ice sheets reached their maximum extent prior to the onset of deglaciation, large parts of their margins would have formed marine-based termini. This configuration would have made their grounding lines highly sensitive to sea-level rise and oceanic warming (Pritchard *et al.* 2012), especially after the start of the last deglaciation from 19 ka onwards (Clark *et al.* 2009; Livingstone *et al.* 2012).

Foraminifera in core PC466 are surprisingly rare during the Holocene when temperatures were significantly warmer and sea ice reduced relative to the last glacial period. The low shell weight (5 μg) found for Holocene-aged planktonic foraminifera contrasts with an average of 12 μg during MIS3, suggesting that the main control on carbonate content during the Holocene was dissolution rather than lack of production or dilution. Sediments deposited during the Holocene also contain large amounts of agglutinated benthic foraminifera and only rare benthic calcareous shells. Holocene dissolution would have been driven by lower carbonate ion concentration in the deep water or within sediment pore water, perhaps related to high fluxes of organic carbon from surface-water productivity (e.g. Wollenburg & Kuhnt 2000).

The maximum in IRD abundance for the core is observed in the top few centimetres of the trigger core, indicating either that the IRD delivery was at a maximum during the latest part of the Holocene or that the core-top sediments were affected by strong current winnowing or increased bioturbation during recent times (Singer & Anderson 1984). An ice-core record from James Ross Island reveals rapid warming in the latest part of the Holocene, especially during the past 50 years, that was associated with collapse of ice shelves and accelerating glacier mass loss in West Antarctica (Mulvaney *et al.* 2012). The IRD maximum observed in the top few centimetres of TC466 may record similar recent climate changes in the Antarctic Peninsula region.

## Conclusions

One of the challenges of working on marine cores from this area is dating sediment with very low carbonate content. We constructed an age model using relative palaeointensity (RPI) and stable isotope stratigraphy, in concert with complementary lithological, sedimentological (IRD, magnetic susceptibility) and quantitative micropalaeontological data. Because the sediments used in this study contained only a very small coarse fraction no additional subsampling was needed to undertake the point counting (IRD, planktonic foraminifera). Therefore, the record has a remarkably small error in comparison to sites, which present large samples. However, extracting useful data on such tiny samples requires both careful handling, and detailed micropalaeontological and sedimentological analyses of all the samples.

Our results suggest that it is possible to date and extract a long palaeoenvironmental record from shallow water depths (i.e. *c.* 2300 m) from the sediment drifts off West Antarctica with IODP drilling. In glacial-aged sediments from core PC466, foraminifera are rare in MIS4, abundant and well preserved in MIS3, and virtually absent from MIS2. Millennial-scale peaks in planktonic foraminifera abundance (and preservation) observed during MIS3 either coincide with or occur slightly after Antarctic warm events in the EDML ice core, indicating either reduced sea-ice cover and/or increased carbonate preservation at these times. The abundance of IRD increased during the last deglaciation between approximately 19 and 11 ka when sea-level rise destabilized the West Antarctic Ice Sheet and the Antarctic Peninsula Ice Sheet, which had advanced across the shelf during the Last Glacial Maximum. The Holocene is marked by poor carbonate preservation and maximum IRD concentrations in the core-top, which may be related to recent warming of the Antarctic Peninsula region.

This work was supported by NERC grant NE/I006214/1 (to D.A. Hodell and M.J. Vautravers), the BAS Polar Science for Planet Earth programme (to C.-D. Hillenbrand, J. Smith and R.D. Larter) and US National Science Foundation grant OCE-0850413 and OCE-1014506 (to J.E.T. Channell). We are also grateful for technical support from J. Curtis (stable isotopes analysis), M. Greave (trace elements analysis), S. Crowhurst and B. Bowe (sediments preparations and sortable silt analysis).

## References

ANDERSON, R. F. & FLEISCHER, M. Q. 2011. Deep ocean carbonate chemistry on millennial to Milankovitch time scales. Goldschmidt conference abstract. *Mineralogical Magazine*, **75**, 437.

ANDERSON, J. B., SHIPP, S. S., LOWE, A. L., WELLNER, J. S. & MOSOLA, A. B. 2002. The Antarctic Ice Sheet during the Last Glacial Maximum and its subsequent retreat history: a review. *Quaternary Science Reviews*, **21**, 49–70.

ANTONOV, J. I., LOCARNINI, R. A., BOYER, T. P., MISHONOV, A. V. & GARCIA, H. E. 2006. *In*: LEVITUS, S. (ed.) *World Ocean Atlas 2005*, *Volume 2*. NOAA Atlas NESDIS, **62**. US Government Printing Office, Washington, DC.

ARRIGO, K., WORTHEN, D. L., DIXON, P. & LIZOTTE, M. P. 1998. Primary productivity of near surface communities within Antarctic pack ice. *In*: LIZOTTE, M. P. & ARRIGO, K. (eds) *Antarctic Sea Ice Biological Processes, Interactions and Variability*. American Geophysical Union, Antarctic Research Series, **73**, 23–43.

BARKER, S., GREAVES, M. & ELDERFIELD, H. 2003. A study of cleaning procedures used for foraminiferal Mg/Ca palaeothermometry. *Geochemistry, Geophysics, Geosystems*, **4**, 9, http://dx.doi.org/10.1029/2003GC000559.

BINDSCHADLER, B. 2006. The environment and evolution of the west Antarctic ice sheet: setting the stage. *Philosophical Transactions of the Royal Society London, Series A*, **364**, 1583–1605.

CHANNELL, J. E. T., XUAN, C. & HODELL, D. A. 2009. Stacking palaeointensity and oxygen isotope data for the last 1.5 Myrs (PISO-1500). *Earth and Planetary Science Letters*, **283**, 14–23.

CLARK, P. U., DYKE, A. S. *ET AL.* 2009. The last glacial maximum. *Science*, **325**, 710–714.

DAVIES, B. J., HAMBREY, M. J., SMELLIE, J. L., CARRIVICK, J. L. & GLASSER, N. F. 2012. Antarctic Peninsula Ice Sheet evolution during the Cenozoic Era. *Quaternary Science Reviews*, **31**, 30–66.

DE VILLIERS, S., GREAVES, M. & ELDERFIELD, H. 2002. An intensity ratio calibration method for the accurate determination of Mg/Ca and Sr/Ca of marine carbonates by ICP-AES. *Geochemistry, Geophysics, Geosystems*, **3**, 1001.

DIECKMANN, G. S., SPINDLER, M., LANGE, M. A., ACKLEY, S. F. & EICKEN, H. 1991. Antarctic sea ice: a habitat for the foraminifer *Neogloboquadrina pachyderma*. *Journal of Foraminiferal Research*, **21**, 182–189.

DONG, S., SPRINTALL, J. & GILLE, S. T. 2006. Location of the Antarctic Polar Front from AMSR-E Satellite Sea Surface Temperature Measurements. *Journal of Physical Oceanography*, **36**, 2075–2089.

DUCKLOW, H. W., BAKER, K. *ET AL.* 2007. Marine pelagic ecosystems: the West Antarctic Peninsula. *Philosophical Transactions of the Royal Society B. Biological Sciences*, **362**, 67–94.

DUCKLOW, H. W., ERICKSON, M. *ET AL.* 2008. Particle export from the upper ocean over the continental shelf of the west Antarctic Peninsula: a long-term record, 1992–2007. *Deep-Sea Research. Part I. Topical Studies in Oceanography*, **55**, 2118–2131.

DREWRY, D. J. 1983. *Antarctica: Glaciological and Geophysical Folio*. Scott Polar Research Institute, Cambridge.

EPICA COMMUNITY MEMBERS. 2006. One-to-one coupling of glacial climate variability in Greenland and Antarctica. *Nature*, **444**, 195–198.

GLADSTONE, R. M., BIGG, G. R. & NICHOLLS, K. W. 2001. Icebergs trajectory modeling and meltwater injection in the Southern Ocean. *Journal of Geophysical Research*, **106**, 19,903–19,915.

HILLENBRAND, C.-D. & EHRMANN, W. 2003. Distribution of clay minerals in drift sediments on the continental rise west of the Antarctic Peninsula, ODP Leg 178, Sites 1095 and 1096. *In*: BARKER, P. F., CAMERLENGHI, A., ACTON, G. D. & RAMSAY, A. T. S. (eds) *Proceedings of ODP Science Results*, **178**. Ocean Drilling Program, College Station, TX, 1–29.

HILLENBRAND, C.-D. & EHRMANN, W. 2005. Late Neogene to Quaternary environmental changes in the Antarctic Peninsula region: evidence from drift sediments. *Global and Planetary Change*, **45**, 165–191.

Hillenbrand, C.-D., Grobe, H., Dieckmann, B., Kuhn, G. & Fütterer, D. K. 2003. Distribution of clay minerals and proxies for productivity in surface sediments of the Bellingshausen and Amundsen seas (West Antarctica): Relation to modern environmental conditions. *Marine Geology*, **193**, 253–271.

Hillenbrand, C.-D., Moreton, S. G. *et al.* 2008*a*. Volcanic time-markers for Marine Isotopic Stages 6 and 5 in Southern Ocean sediments and Antarctic ice cores: implications for tephra correlations between palaeoclimatic records. *Quaternary Science Reviews*, **27**, 518–540.

Hillenbrand, C.-D., Camerlenghi, A., Cowan, E. A., Hernandez-Molina, F. J., Lucchi, R. G., Rebesco, M. & Uenzelmann-Neben, G. 2008*b*. The present and past bottom-current flow regime around the sediment drifts on the continental rise west of the Antarctic Peninsula. *Marine Geology*, **255**, 55–63.

Hillenbrand, C.-D., Smith, J. A. *et al.* 2010. Age Assignment of a diatomaceous ooze deposited in the western Amundsen Sea Embayment after the last Glacial Maximun. *Journal of Quaternary Science*, **25**, 280–295.

Ito, T., Woloszyn, M. & Mazloff, M. 2010. Anthropogenic carbon dioxide transport in the Southern Ocean driven by Ekman flow. *Nature*, **463**, 80–83, http://dx.doi.org/10.1038/nature08687.

Joughin, I. & Alley, R. B. 2011. Stability of the West Antarctic ice sheet in a warming world. *Nature Geoscience*, **4**, 506–513, http://dx.doi.org/10.1038/NGEO1194.

Kanfoush, S. L., Hodell, D. A., Charles, C. D., Guilderson, T. P., Mortyn, G. & Ninnemann, U. S. 2000. Millennial-scale instability of the Antarctic ice sheet during the last glaciation. *Science*, **288**, 1815; doi: 10.1126/science.288.5472.1815.

Kohfeld, K. E., Fairbanks, R. G., Smith, S. L. & Walsh, I. D. , 1996. Neogloboquadrina pachyderma (sinistral coiling) as paleoceanographic tracers in polar oceans: evidence from Northeast Polynya plankton tows, sediment traps, and surface sediments. *Paleoceanography*, **11**, 679–699.

Kwok, R. & Comiso, J. C. 2002. Southern Ocean climate and sea ice anomalies associated with the Southern Oscillation. *Journal of Climate*, **15**, 487–501.

Livingstone, S. J., Ó Cofaigh, C., Stokes, C. R., Hillenbrand, C.-D, Vieli, A. & Jamieson, S. R. 2012. Antarctic palaeo-ice streams. *Earth Science Reviews*, **111**, 90–128, http://dx.doi.org/10.1016/j.earscirev.2011.10.003.

Locarnini, R. A., Mishonov, A. V., Antonov, J. I., Boyer, T. P. & Garcia, H. E. 2006. *In*: Levitus, S. (ed.) *World Ocean Atlas 2005, Volume 1*. NOAA Atlas NESDIS, **61**. US Government Printing Office, Washington, DC.

Lucchi, R. G. & Rebesco, M. 2007. Glacial contourites on the Antarctic Peninsula margin: insight for palaeoenvironmental and palaeoclimatic conditions. *In*: Viana, A. R. & Rebesco, M. (eds) *Economic and Palaeoceanographic Significance of Contourite Deposits*. Geological Society, London, Special Publications, **276**, 111–127.

Lucchi, R. G., Rebesco, M., Busetti, M., Caburlotto, A., Colizza, E. & Fontolan, G. 2002. Mid-late Pleistocene glacimarine sedimentary processes of a high-latitude, deep- sea sediment drift (Antarctic Peninsula Pacific margin). *Marine Geology*, **189**, 343–370.

Mackensen, A., Grobe, H., Hubberten, H-W. & Kuhn, G. 1994. Benthic foraminiferal assemblages and the $\delta^{13}C$ signal in the Atlantic sector of the Southern Ocean: glacial to interglacial contrast. *In*: Zahn, R. (ed.) *Carbon Cycling in the Glacial Ocean: Constraints on the Ocean's Role in Global Change*. NATO ASI Series, **17**, 105–145.

Macri, P., Sagnotti, L. & Lucchi, R. G. 2006. A stacked record of relative geomagnetic palaeointensity for the past 270 kyr from the western continental rise of the Antarctic Peninsula. *Earth Planetary Science Letter*, **252**, 162–179.

Martinson, D. G., Stammerjohn, S. E., Iannuzzi, R. A., Smith, R. C. & Vernet, M. 2008. Western Antarctic Peninsula physical oceanography and spatio-temporal variability. *Deep-Sea Research Part II. Topical Studies in Oceanography*, **55**, 1964–1987.

Mayewski, P. A., Meredith, M. P. *et al.* 2009. State of the Antarctic and Southern Ocean climate system. *Reviews of Geophysics*, **47**, RG1003, http://dx.doi.org/10.1029/2007RG000231.

McCave, I. N. & Hall, I. R. 2006. Size sorting in marine muds: processes, pitfalls, and prospects for palaeoflow-speed proxies. *Geochemistry, Geophysics, Geosystems*, **7**, 10, http://dx.doi.org/10.1029/2006GC001284.

McCave, I. N., Manighetti, B. & Robinson, S. G. 1995. Sortable silt and fine sediment size/composition slicing: parameters for palaeocurrent speed and palaeoceanography. *Palaeoceanography*, **10**, 593–610.

Mercer, J. H. 1978. West Antarctica Ice sheet and $CO_2$ Greenhouse effect. Threat of disaster. *Nature*, **271**, 321–325.

Meredith, M. P. & King, J. C. 2005. Rapid climate change in the ocean west of the Antarctic Peninsula during the second half of the 20th century. *Geophysical Research Letter*, **32**, L19604, http://dx.doi.org/10.1029/2005GL024042.

Mleneck-Vautravers, M. J. 1997. *Sédimentation et dissolution des carbonates biogéniques aux moyennes latitudes Nord et Sud*. PhD thesis, University Bordeaux I.

Moy, A. D., Howard, W. R., Bray, S. G. & Trull, T. W. 2009. Reduced calcification in modern Southern Ocean planktonic foraminifera. *Nature Geoscience*, **2**, 276–280.

Mulitza, S., Donner, B., Fischer, G., Paul, A., Pätzold, J., Rühlemann, C. & Segl, M. 2004. The South Atlantic oxygen isotope record of planktic foraminifera. *In*: Wefer, G., Mulitza, S. & Ratmeyer, V. (eds) *The South Atlantic in the Late Quaternary*. Springer, Berlin, 121–142.

Mulvaney, R., Abram, N. J. *et al.* 2012. Recent Antarctic Peninsula warming relative to Holocene climate and ice-shelf history. *Nature*, **489**, 141–144, http://dx.doi.org/10.1038/nature11391.

Orsi, A. H., Whitworth, T. & Nowlin, W. D. 1995. On the Meridional extent and fronts of the Antarctic

Circumpolar Current. *Deep-Sea Research Part I. Topical Studies in Oceanography*, **42**, 641–673.

Parkinson, C. L. 2004. Southern Ocean sea ice and its wider linkages; insights revealed from models and observations. *Antarctic Science*, **16**, 387–400.

Pritchard, H. D., Arthern, R. J., Vaughan, D. G. & Edwards, L. A. 2009. Extensive dynamic thinning on the margins of the Greenland and Antarctic ice sheets. *Nature*, **461**, 971–975.

Pritchard, H. D., Ligtenberg, S. R. M., Fricker, H. A., Vaughan, D. G., van den Broeke, M. R. & Padman, L. 2012. Antarctic ice-sheet loss driven by basal melting of ice shelves. *Nature*, **484**, 502–505.

Pudsey, C. J. 2000. Sedimentation on the continental rise west of the Antarctic Peninsula over the last three glacial cycles. *Marine Geology*, **167**, 313–338.

Pudsey, C. J. & Camerlenghi, A. 1998. Glacial-interglacial deposition on a sediment drift on the Pacific margin of the Antarctic Peninsula. *Antarctic Science*, **10**, 286–308.

Rasmussen, S. O., Seierstad, I. K., Andersen, K. K., Bigler, M., Dahl-Jensen, D. & Johnsen, S. J. 2008. Synchronization of the NGRIP, GRIP, and GISP2 ice cores across MIS2 and palaeoclimatic implications. *Quaternary Science Reviews*, **27**, 18–28, http://dx.doi.org/10.1016/j.quascirev.2007.01.016.

Rebesco, M., Pudsey, C. J., Canals, M., Camerlenghi, A., Barker, P., Estrada, F. & Giorgetti, A. 2002. Sediment drift and deep-sea channel systems, Antarctic Peninsula Pacific margin. *In*: Stow, D. A. V., Pudsey, C. J., Howe, J. A., Faugeres, J. C. & Viana, A. R. (eds) *Deep-Water Contourite Systems: Modern Drifts and Ancient Series, Seismic and Sedimentary Characteristics*. Geological Society, London, Memoirs, **22**, 353–371.

Rickaby, R. E. M., Elderfield, H., Roberts, N., Hillenbrand, C. D. & Mackensen, A. 2010. Evidence for elevated alkalinity in the glacial Southern Ocean. *Palaeoceanography*, **25**, PA1209, http://dx.doi.org/10.1029/2004GC000858.

Sagnotti, L., Macrì, P., Camerlenghi, A. & Rebesco, M. 2001. Environmental magnetism of Antarctic late Pleistocene sediments and interhemispheric correlation of climatic events. *Earth and Planetary Sciences Letter*, **192**, 65–80.

Siddall, M., Rohling, E. J., Thompson, W. G. & Waelbroeck, C. 2008. Marine isotopic stage 3 sea level fluctuations: data synthesis and new outlook. *Reviews of Geophysics*, **46**, RG4003, http://dx.doi.org/10.1029/2007RG000226.

Singer, J. K. & Anderson, J. B. 1984. Use of total grain-size distributions to define bed erosion and transport for poorly sorted sediment undergoing simulated bioturbation. *Marine Geology*, **57**, 335–359.

Thomas, R. G., Guyodo, Y. & Channell, J. E. T. 2003. U channel track for susceptibility measurements. *Geochemistry, Geophysics, Geosystems*, **4**, 1050, http://dx.doi.org/10.1029/2002GC000454.

Vaughan, D. G., Marshall, G. J. *et al.* 2003. Recent rapid regional climate warming on the Antarctic Peninsula. *Climatic Change*, **60**, 243–274.

Villa, G., Persico, D., Bonci, M. C., Lucchi, R. G., Morigi, C. & Rebesco, M. 2003. Biostratigraphic characterization and Quaternary microfossil palaeoecology in sediment drifts west of the Antarctic Peninsula – implications for cyclic glacial-interglacial deposition. *Palaeogeography, Palaeoclimatology, Palaeoecology*, **198**, 237–263.

Venuti, A., Florindo, F. *et al.* 2011. Late Quaternary sediments from deep-sea sediment drifts on the Antarctic Peninsula Pacific margin: climatic control on provenance of minerals. *Journal of Geophysical Research, B*, **116**, B06104, http://dx.doi.org/10.1029/2010JB007952.

Vilkes, G. 1975. Comparison of Globorotalia Pachyderma (Ehrenberg) in the water column and sediments of the Canadian Arctic. *Journal of Foraminiferal Research*, **5**, 313–325.

Wefer, G., Fischer, G., Fuetterer, D. & Gersonde, R. 1988. Seasonal particle flux in the Bransfield Strait, Antartica. *Deep Sea Research Part A. Oceanographic Research Papers*, **35**, 891–898.

Withworth, T., III, Orsi, A. H., Kim, S.-J. & Nowlin, W. D., Jr. 1998. Water masses and mixing near the Antarctic Slope Front. *In*: Jacobs, S. & Weiss, R. (eds) *Ocean Ice and Atmosphere Interactions at the Antarctic Continental Margin*. American Geophysical Union, Antarctic Research Series, **75**, 1–27.

Wolff, E. W., Fischer, H. *et al.* 2006. Southern Ocean sea-ice extent, productivity and iron flux over the past eight glacial cycles. *Nature*, **440**, 491–496, http://dx.doi.org/10.1038/nature04614.

Wollenburg, J. E. & Kuhnt, W. 2000. The response of benthic foraminifers to carbon flux and primary production in the Arctic Ocean. *Marine Micropalaeontology*, **40**, 189–231.

Young, N. W. 1998. Antarctic iceberg drift and ocean currents derived from scatterometer image series. *In*: *European Space Agency Work Emerging Scatterometer Applications*. ESA Publications Division, ESA SP-424, 125–132.

Yuan, X. 2004. ENSO-related impacts on Antarctic sea ice: a synthesis of phenomenon and mechanisms. *Antarctic Science*, **16**, 415–425.